SPE 95952

Deepwater Reservoir Modeling Using Sequence-Stratigraphic and Geomorphic Constraints

M.J. Pranter, SPE, Z.A. Reza, SPE, and P. Weimer, U. of Colorado

This paper was prepared for presentation at the 2005 SPE Annual Technical Conference and Exhibition held in Dallas, Texas, U.S.A., 9 – 12 October 2005.

Abstract

In deepwater-reservoir modeling, it is important to properly represent the spatial distribution of architectural elements to account for pore-volume distribution and the connectivity of reservoir sand bodies. This is especially critical for rock and fluid-volume estimates, reservoir-performance predictions, and development-well planning.

This new integrated stochastic reservoir-modeling approach accounts for stratigraphic and geomorphic controls to generate the reservoir architecture. Information on stratal-package evolution and sediment provenance can be integrated into the reservoir-modeling process. A slope-area analytical approach is implemented to account for topographical constraints on channel and sheet-form reservoir architectures and their distribution. Inferred paleo-channel direction statistics (from outcrop and stratigraphic studies) and simulated high-frequency eustatic sea-level curves are also used to constrain the architectural-element statistics. Based on these geomorphic and sedimentological constraints, architectural elements (channels, lobes, sheets) are built into the model sequentially (in age order).

Integration of realistic geological and engineering attributes into numerical reservoir models is vital for optimal reservoir management. This approach is unique in that it is constrained more directly to geomorphic and sedimentological parameters than traditional object-based or surface-based techniques for stochastic deepwater reservoir modeling.

Introduction

Our understanding of the reservoir architecture of deepwater systems has improved with recent advances in imaging of the shallow and deep subsurface and through characterization with outcrop analogs. However, we do not have a complete knowledge of the subsurface environment, so a high degree of uncertainty remains when building deepwater-reservoir models. Stochastic-modeling approaches are useful because they provide a means of quantifying uncertainty through generation of multiple realizations of reservoir-property models. A number of stochastic modeling techniques are presently available for building deepwater reservoir models that can be broadly classified into three categories: (1) *cell-based* approaches that primarily implement two-point geostatistics[1], and more recently multipoint geostatistical concepts[2]; (2) o*bject-based* or *Boolean* approaches have been used to build more geologically realistic reservoir models that incorporate nonlinear features[3,4,5]. The geologic objects are conditioned to hard data (e.g. wells) and also honor stratigraphic relationships and interpretations; (3) *stochastic surface-based* techniques[6,7] have been used to capture the compensational stacking tendency of flow-event deposits within deepwater lobes.

In contrast to stochastic methods, process-based methods attempt to simulate fundamental geological processes to produce a numerical representation of the reservoir geology[8,9]. These approaches include the rigor of the physics of sedimentation and depositional processes. However, enormous difficulties arise when it comes to conditioning process-based models to existing data (e.g., honoring well and seismic data).

We introduce a novel approach to deepwater reservoir modeling that has aspects of process-based techniques but is also related to stochastic surface-based methods. A combination of concepts is adopted in this approach to honor geomorphic and stratigraphic constraints. In this paper, geomorphic refers to bathymetry and parameters derived from bathymetry. To identify flow paths for deepwater channels and lobes, concepts from hypsometric analysis of channelized flow are incorporated. The spatial variability in deepwater architecture that is common within a sequence-stratigraphic framework is incorporated through inputs

for initial bathymetry, sediment-source location, channel and lobe (sheet) dimensions, channel erosion/deposition, and other controls that can vary stratigraphically.

Methodology

The developed deepwater-reservoir-modeling approach attempts to incorporate geomorphic and stratigraphic constraints. The deposition of deepwater channels, lobes (sheets), and condensed sections (or hemipelagic shale) is simulated in this approach (Fig. 1). In this modeling approach, one channel and associated lobe are simulated at one time and the deepwater stratigraphy is constructed starting at the base (initial bathymetric surface) of the model domain and built upward through the model domain through successive modeling of channel-lobe and condensed section deposits. Thus, the algorithm proceeds with an interpreted initial bathymetry (for example, from 3D seismic data) upon which deposition of the channels and lobes stack to produce the desired stratigraphic architecture. The bathymetry of an area is a function of the local and regional structure, stratigraphy, and other factors. Bathymetry is important because it affects sedimentation. In this approach, we assume that an interpretation of the initial bathymetric surface is complete. This approach can be used to model multiple realizations of deepwater reservoirs using different interpretations of the initial bathymetric surface. The model domain could represent the scale of deposits within a confined intraslope minibasin as well as an unconfined deepwater setting. The orientation, length, sinuousity, and dimensions of the channel are controlled by the initial and subsequent bathymetric surfaces and other constraints that are discussed.

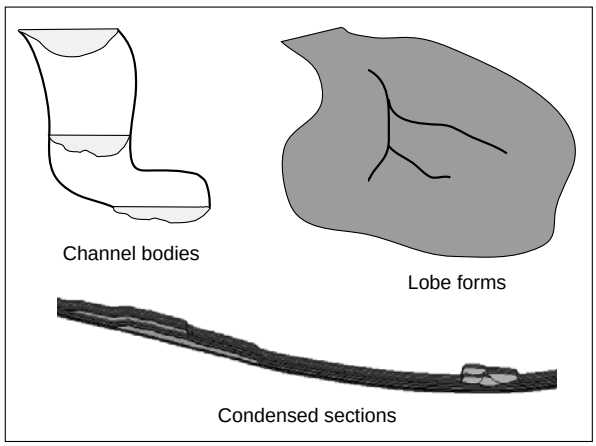

Figure 1: Schematic illustration of deepwater reservoir elements that are modeled using this approach.

The process of modeling deepwater reservoir elements and architecture has several steps. We defined reservoir element as a part of a reservoir characterized by unique stratigraphic and petrophysical properties that distinguishes it from other parts of a reservoir (e.g., channel or lobe). Reservoir architecture refers to the spatial arrangement and geometry of reservoir elements (e.g., lateral continuity and stacking of sedimentary deposits). We start with the geomorphic parameterization of the initial bathymetric surface (or as it exists in any arbitrary time). The goal is to compute several parameters that are used to constrain the placement of the reservoir architectural elements. Then, the channel-entry point or starting grid cell of the channel into the basin is determined. After the channel-entry point is selected, our next steps attempt to answer the following questions through the modeling process: (1) where and how will the channels be placed? (2) how much erosion exists at the base of the channel? and (3) what are the geometries of the channel and channel-fill deposits? Once the channels and channel-fill deposits are modeled, similar modeling strategies are used for placing the deepwater lobes (sheets). Finally, a thin hemipelagic shale interval or condensed section can be modeled based on the concept of pelagic or hemipelagic sedimentation in deepwater settings. A detailed description of each of these steps follows.

Geomorphic Parameterization. The geometry and distribution of deepwater channels, channel fills, and lobes (sheets) vary considerably in response to changes in gradient of the bathymetric surface, so characteristics of the bathymetry are considered. Several geomorphic parameters are evaluated using the initial and subsequent post-depositional bathymetric surfaces. Of these, the sediment-flow vector and contributing area of each grid cell are computed first (Figs. 2 and 3). We define the sediment-flow vector as the vector representation of the likely direction of the sediment flow. It has a slope and direction (azimuth) associated with it and is computed from the bathymetry. The contributing area refers to the value assigned to a grid cell that represents the amount of upslope area that can contribute to sediment transport to that cell (all upslope cells that can contribute; not only adjacent-upslope cells).

First consider the sediment-flow vector. We use a modified version of the D_∞ multiple flow direction model as presented by Tarboton[10] to calculate sediment-flow vectors across the initially interpreted and subsequently computed bathymetric surfaces. This procedure represents flow direction as a vector in the direction of the steepest downward slope on eight triangular facets centered at each grid cell (Fig. 2). An infinite number of flow directions is possible having angles between between 0 and 360^o (thus the symbol D_∞). The two downslope grid cells closest to the vector flow angle share the flow from a grid cell on the basis of angle proportioning as indicated in Fig. 2C.

Calculation of the sediment-flow vector is as follows (modified from Tarboton[10]). For all grid cells, pointers 1 to 8 are assigned to adjacent cells for

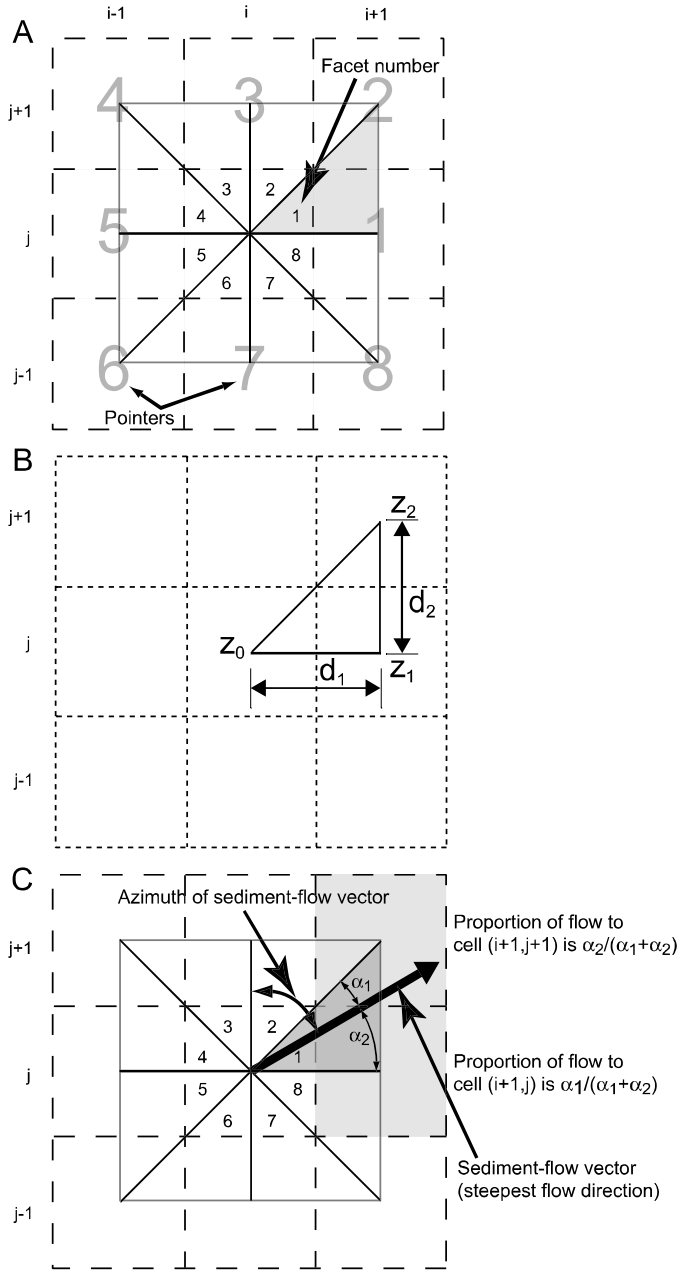

Figure 2: Schematic diagram to illustrate several components to compute sediment-flow path as part of the geomorphic parameterization. a) Relationship between the global grid cell and local facet indexing sediment-flow path computation. Table 2 lists the projections from the global to local indices (and vice versa). b) Bathymetry and distance variables to compute the slope and angle for one facet (in this case, facet 1). c) Illustration to show the proportioning of flow to adjacent grid cells. The two cells [(i+1, j+1) and (i+1, j)] that are highlighted in gray will receive sediment flow from the central grid cell (i, j). Modified from Tarboton[10].

referencing (Fig. 2A). Pointers are used during the modeling process for various referencing reasons. Eight triangular facets exist between a grid cell and its eight adjacent cells in a 3 x 3 grid cell window (Fig. 2A). Each of these facets has one downslope vector with the maximum angle of descent. The outward projection of this downslope vector from the center of the grid cell will lie within or outside the facet of interest. If the downslope vector lies outside the facet, then the angle between the vector and the adjacent facet margin cannot exceed 45°, and the sediment-flow direction for that facet is assigned the direction of the adjacent facet edge. The sediment-flow vector assigned to the grid cell is the steepest of the downslope vectors among the eight facets. For a single triangular facet (Fig. 2B), downward slope is represented by the vector (s_1, s_2) where

$$s_1 = (z_0 - z_1)/d_1 \qquad \ldots (1)$$

$$s_2 = (z_1 - z_2)/d_2 \qquad \ldots (2)$$

where z_i and d_i are bathymetry and distance values between grid cells indicated in Fig. 1. The slope direction and magnitude are computed using

$$r = \tan^{-1}(s_2/s_1) \qquad s = \sqrt{s_1^2 + s_2^2} \qquad \ldots (3)$$

If r is not in the range $(0, \tan^{-1}(d_2/d_1))$ then r is set as the direction along the appropriate edge and s assigned as the slope along that edge, as

$$\text{If} \quad r < 0, \quad set \quad r = 0, \quad s = s_1$$

$$\text{If} \quad r > \tan^{-1}(d_2/d_1), \quad set \quad r = \tan^{-1}(d_2/d_1), \quad s = (z_0 - z_1)/\sqrt{d_1^2 + d_2^2} \qquad \ldots (4)$$

Mapping of any facet bathymetry and distance values to corresponding values on the eight-facet system (Fig. 2) is arranged such that z_0 is the center point, z_1 is the lateral point, and z_2 is the diagonal point of each facet. The local angle corresponding to the largest downward slope of the eight facets ($r'=r$ with maximum s) is converted to azimuth to obtain the sediment flow direction using the following equation

$$r_g = \alpha_f r' + \alpha_c \pi/2 \qquad \ldots (5)$$

where α_f and α_c are defined in Table 1 for the eight facets. Table 1 values differ from Tarboton (1997) because of the definition of the azimuth and coordinate orientation adopted in this work.

The goal of using contributing area in this modeling approach is that it identifies the likelihood that sedimentation could take place at a cell based on the amount of the upslope area that could contribute sediment to that cell location. The greater the contributing area of a grid cell, the more likely that depositional events will occur in that cell. To compute contributing area for a cell, all upslope cells that contribute to deposition to the cell are included. Thus, the contributing area to each grid cell, $a(i,j)$, is evaluated by

$$a(i,j) = \Delta + \sum_{k \text{ contributing adjacent cells}} p_k a(i_k, j_k) \qquad \ldots (6)$$

Facet	z_0	z_1	z_2	α_c	α_f
1	$z_{i,j}$	$z_{i+1,j}$	$z_{i+1,j+1}$	1	-1
2	$z_{i,j}$	$z_{i,j+1}$	$z_{i+1,j+1}$	0	1
3	$z_{i,j}$	$z_{i,j+1}$	$z_{i-1,j+1}$	4	-1
4	$z_{i,j}$	$z_{i-1,j}$	$z_{i-1,j+1}$	3	1
5	$z_{i,j}$	$z_{i-1,j}$	$z_{i-1,j-1}$	3	-1
6	$z_{i,j}$	$z_{i,j-1}$	$z_{i-1,j-1}$	2	1
7	$z_{i,j}$	$z_{i,j-1}$	$z_{i+1,j-1}$	2	-1
8	$z_{i,j}$	$z_{i+1,j}$	$z_{i+1,j-1}$	1	1

Table 1: Global grid cell and local facet indexing for local to global mapping of the parameters in the slope calculation (modified from Tarboton, 1997).

where p_k is the proportion of flow from the adjacent grid cell k that contributes to the grid cell (i,j); Δ is area of each grid cell. Note that Equation 6 is a recursive equation; all upstream cells are considered. The proportion of flow, p_k, for each adjacent grid cell is determined as indicated in Fig. 2C. An example of the contributing area calculation is provided in Fig. 3.

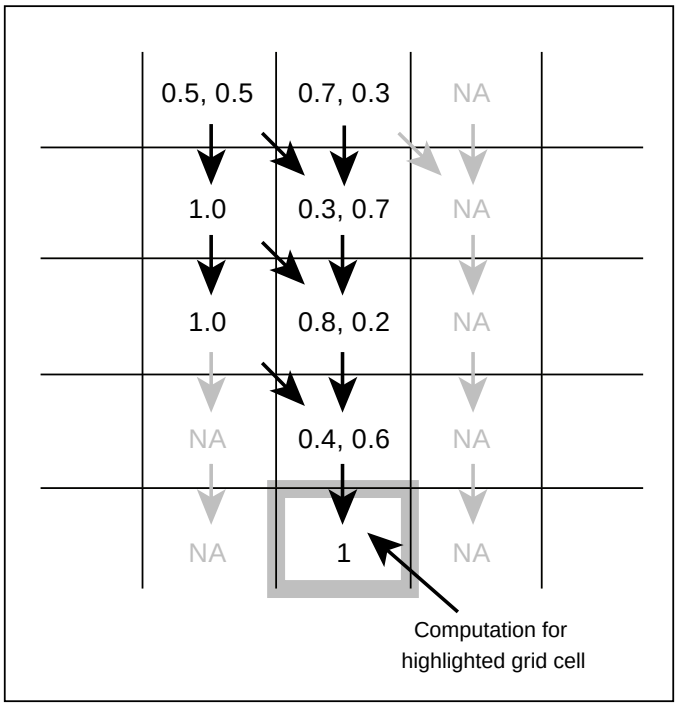

Figure 3: Schematic diagram to illustrate the computation of contributing area as part of the geomorphic parameterization. This contributing area is calculated for the cell highlighted by the bold gray rectangle. The numbers in each grid cell correspond to the proportion of flow coming from the adjacent upslope grid cell(s). The arrows show the sediment-flow path directions. The black arrows correspond to grid cells that contribute sediment flow to the highlighted grid cell (i.e., they are part of the upslope area for the highlighted grid cell). The gray arrows correspond to grid cells that do not contribute sediment flow to the highlighted grid cell. NA=not applicable.

Channel-Entry Point. During the modeling process, deepwater channel and lobe reservoir elements are modeled with each channel beginning on the edge of the model domain. The entry point for a channel (channel-entry point) on the margin of the model domain is determined stochastically from a histogram of channel-entry point azimuths that indicate the direction from which a channel originates. Several rules are honored during the selection of a channel-entry point location. The channel-entry point from which a channel reservoir element originates is determined by, first, randomly selecting the azimuth for the proposed location from an input histogram (Fig. 4). The azimuth is determined from an origin in the center of the model domain (e.g., an azimuth of 90° indicates that the channel will originate on the model edge due east). The final channel-entry point location is selected from within a tolerance window

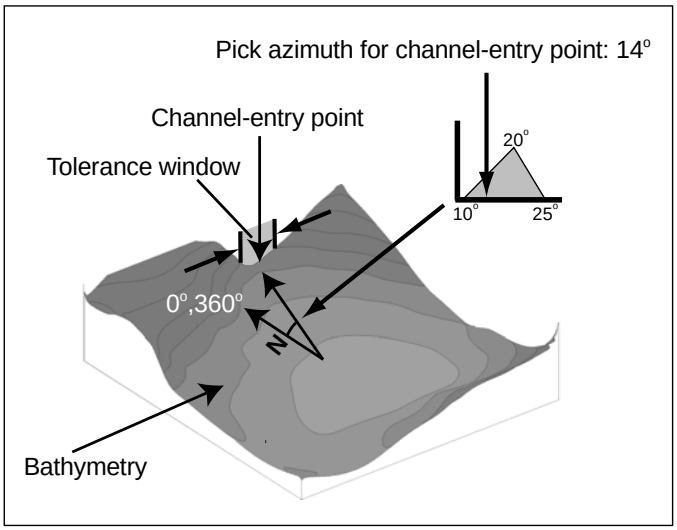

Figure 4: Schematic diagram that illustrates the selection of the channel-entry point. The channel-entry point from which a channel reservoir element originates is determined by, first, randomly selecting the azimuth for the proposed location from an input histogram. The final channel-entry point location is selected from within a tolerance window surrounding the proposed location for the channel-entry point.

surrounding the proposed location for the channel-entry point. Within the tolerance window, pointers (calculated previously in geomorphic parameterization) for all the grid cells are checked as to whether the downward slope direction points into the model domain. For all grid cells that have downward slope directions into the model domain, the grid cell with the lowest elevation is picked as the starting point (channel-entry point) of the channel trajectory.

Sequence-Stratigraphic Controls. A number of sequence-stratigraphic controls are integrated into the modeling approach. The architectural elements that are modeled include single-story channels (that can stack into channel complexes), accompanying deepwater lobes (sheets), and condensed sections. The channels can be

erosional, depositional, or a combination of both erosional and depositional[11]. Updip-to-downdip aspect ratios (width-to-thickness ratios) of the channel fills range from as low as 10:1 to approximately 50:1. Channel width increases downdip for all channels.

Channel erosion occurs along the length of the channel and stops when the channel trajectory encounters a mean gradient value that is less than a specified threshold (e.g., 1.0°). The threshold value can vary depending on geological information of the sea floor, substrate, and depositional processes of a particular area. Where channel erosion ends, the channel becomes depositional in nature. Channel erosion is the maximum at the updip location. Erosion decreases basinward to zero at the erosion termination point in the channel. Erosion generally decreases across the channel width at any point along a channel trajectory. However, the amount of erosion across the channel width also depends on the local bathymetry. The channel-fill thickness is the same as the erosion thickness at the updip location and decreases downdip. Presently, this approach does not model levees as distinct reservoir elements. Channel-fill thickness decreases across the channel width. The aspect ratio of the deepwater lobes (>500:1) is an order of magnitude greater than that of the channel bodies. Condensed-section thickness is an order of magnitude less than the updip channel-fill thickness. Variability in the initial (updip) channel thickness, channel aspect ratio, and channel-entry point location is honored in the models from one channel-lobe depositional event to another based on the input histograms for these parameters (Fig. 5).

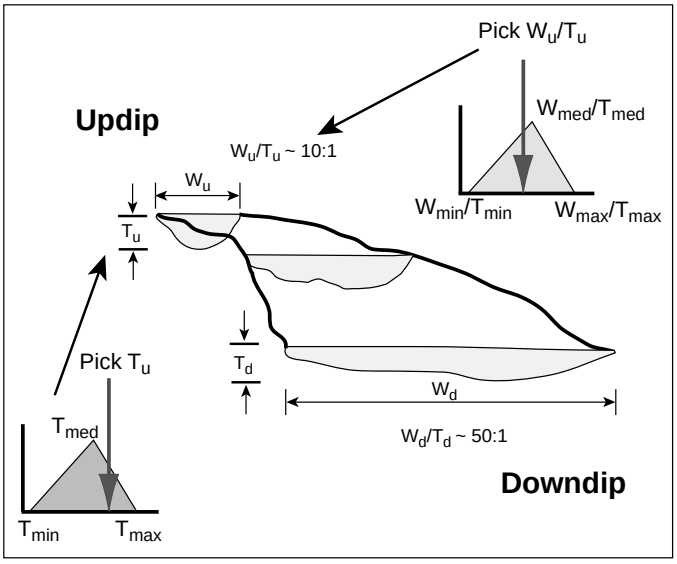

Figure 5: Schematic diagram that illustrates the selection of the initial channel aspect ratio and channel thickness. These initial values are randomly selected from corresponding input triangular histograms. Updip-to-downdip aspect ratios (width-to-thickness ratios) of the channel fills range from as low as 10:1 to approximately 50:1. Channel width increases downdip for all channels. Channel-fill thickness decreases across the channel width.

Channel-Trajectory Determination. Deepwater channels are defined as elongate, negative-relief features produced and/or maintained by turbidity current flow[12]. Channels represent relatively long-term pathways for sediment transport. Channel shape and position within a turbidite system are controlled by depositional processes and erosional downcutting or a combination of both processes[11,12].

The location of a deepwater channel (herein referred to as channel trajectory) in the model domain is determined following several rules. The channel trajectory starts from the channel-entry-point location identified previously. The channel trajectory is then computed for one grid cell at a time and generally in a basinward direction. For each cell along the presently computed channel trajectory, several parameters are computed that can influence the subsequent channel trajectory. These parameters include the tortuosity and curvature of the computed channel trajectory, local slope, mean slope, total bathymetric increase, and instantaneous bathymetric increase. To determine the channel trajectory, adjacents that would result in high values of tortuosity and/or curvature of the channel trajectory are excluded. The four main rules for channel trajectory determination are illustrated in a flow diagram (Fig. 6).

For each grid cell along the channel trajectory, the channel trajectory is directed from the current grid cell toward the cell in the direction of the steepest downward slope (Rule 1, Fig. 6). If, however, the current grid cell of the channel trajectory is deeper than the adjacent grid cells, the channel can still progress if the bathymetric difference between the deepest adjacent grid cell and the current grid cell is less than a threshold value (e.g., equivalent to 10% of the starting channel thickness) (Rule 2). A low threshold reflects a relatively low erosive energy of a deepwater sediment flow. If this rule is not met, then the channel trajectory can still progress to the adjacent grid cell that results in the minimum curvature for the channel trajectory (Fig. 6). The minimum curvature rule (Rule 3) will apply only if the bathymetric difference between the adjacent grid cell and the current grid cell is less than another threshold value (e.g., equivalent to 20% of the starting channel thickness). If rule 3 is not met, then the trajectory can progress to the adjacent cell with the greatest contributing area, if the bathymetric difference between the adjacent grid cell and the current grid cell is less than a greater threshold value than those used in rules 2 and 3 (e.g., equivalent to 25% of the starting channel thickness) (Rule 4).

Along the channel trajectory, the threshold values used in the channel trajectory algorithm, decrease basinward. These rules are used to approximate the erosive energy of the deepwater system. The threshold values decrease basinward to reflect the lower erosive energy of the system. Thus, it becomes more difficult for the channel to progress farther. The channel trajectory terminates when none of the criteria discussed above are encountered.

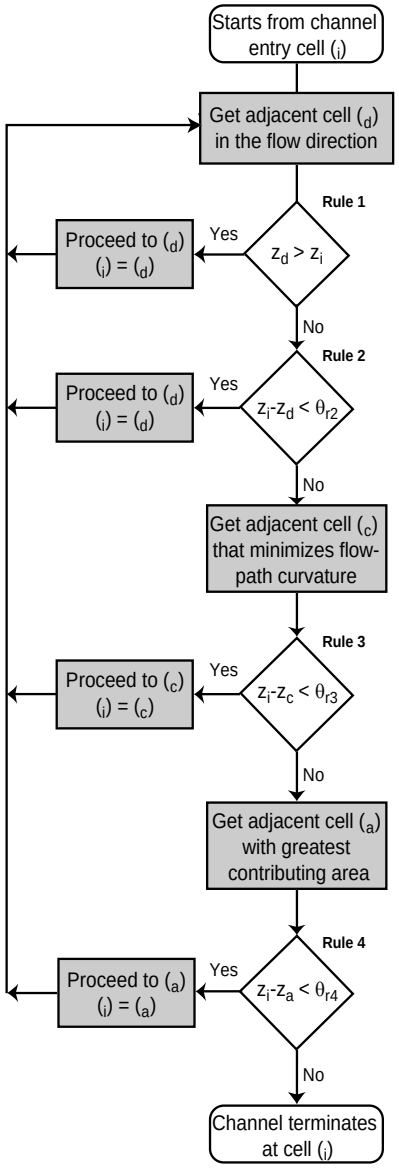

Figure 6: Flow diagram to illustrate the determination of the channel-trajectory. The trajectory starts at the channel-entry point. Four rules (1, 2, 3, 4) are depicted in the flow chart that dictate how the channel trajectory progresses. The variable z is the bathymetry and θ is the bathymetric threshold. Subscripts i, d, c, and a for the variable z denote the bathymetry values for the initial or current grid cell, downslope adjacent cell, adjacent cell based on the curvature rule, and adjacent cell based on contributing area rule, respectively. Subscripts r2, r3 and r4 for the variable θ denote threshold values used in rules 2, 3, and 4, respectively (see text for explanation).

Channel Geometry. The geometries of open channels and filled channels change in response to changes in gradient, from a single deep feeder channel to shallower and broader channels and sets of channels in a more unconfined setting (Weimer and Slatt, 2004). The width and the thickness of the channel along its trajectory are determined using the starting thickness and aspect ratio values, θ_0 and α_0, respectively. These starting thickness and aspect ratio values are randomly drawn from corresponding input histograms. The steps used in the calculation of width and thickness are as follows:
Starting width, w_0, is determined from

$$w_0 = \theta_0 \, \alpha_0 \qquad \ldots (7)$$

Downdip aspect ratio, α_n, is determined using

$$\alpha_n = \alpha_0 \, A_\alpha \qquad \ldots (8)$$

where A_α is the aspect-ratio increase factor, and n is the number of grid cells in the channel trajectory. Downdip width, w_n, is determined using

$$w_n = w_0 \, A_w \qquad \ldots (9)$$

where A_w is width increase factor. Downdip thickness, θ_n, is determined using

$$\theta_n = \theta_0 \, A_\theta \qquad \ldots (10)$$

where A_θ is thickness decrease factor. The factors used in Equations 10 – 12 are not independent of each other. They are related using

$$A_\theta = A_\alpha \big/ A_w \qquad \ldots (11)$$

where only A_α and A_w are supplied, and A_θ is determined from Equation 11. For any grid cell, i, along the channel trajectory, the current aspect ratio is determined by

$$\alpha_i = \alpha_n - \frac{n-i+1}{n}\left(\alpha_n - \alpha_0\right) \qquad i = 1, \ldots, n \qquad \ldots (12)$$

For any grid cell, i, along the channel trajectory, the current channel thickness is determined by

$$\theta_i = \theta_0 - \frac{i-1}{n}\left(\theta_0 - \theta_n\right) \qquad i = 1, \ldots, n \qquad \ldots (13)$$

and the current width is determined by

$$w_i = \theta_i \, \alpha_i \qquad i = 1, \ldots, n \qquad \ldots (14)$$

The end of erosion, n_s, is determined based on a specified mean slope criterion during the channel trajectory determination. The scour amount, $(\theta_s)_i$, of the current grid cell along the channel trajectory up to the scour termination point is determined by

$$\left(\theta_s\right)_i = \left(1 - \frac{i-1}{n_s}\right)\theta_i \qquad i = 1, \ldots, n \qquad \ldots (15)$$

A similar approach is also utilized for lobe distributary thickness and width. However, the aspect ratio of the lobe form bodies is maintained as an order of magnitude greater than that of the channel form bodies. Also, for lobe form bodies, no scour event is simulated.

Deepwater-Lobe Placement. Sheet sands are deposited from decelerating flows at the termini of channels to form deepwater lobes. Sheet sands and sandstones and deepwater lobes reflect the sediments that have bypassed through updip channels (confined flow) and

are deposited in a primarily unconfined setting. They are characterized by high-aspect-ratio reservoir sand bodies (>500:1), which differ markedly in aspect from the updip channels that feed them.

The placement of deepwater lobes is determined using the following approach. The deepwater lobes are modeled at the end of the channel trajectory by using several distributary branches. The distributary branches are used solely as a modeling method to create a deepwater lobe form and are not additional reservoir elements in the model. The distributary branches extend outward in various directions and with various lengths to produce a range of deepwater lobe geometries. To create a lobe form, along the channel trajectory and near the end of the channel, a number of grid cells are identified based on gradient criteria. These grid cells are starting points for the distributary branches. The grid cells are selected where the local and mean gradients of the channel trajectory are less than some threshold values. Similar to the approach to determine the channel trajectory, these distributary branches are systematically advanced into the model, and these trajectories should not intersect with the channel trajectory from which they originate. The lobe form thickness randomly decreases outward from the distributary branches.

After channel-lobe deposition, hemipelagic shale or condensed section deposition can be simulated, when appropriate. The thickness of the hemipelagic shale or condensed section is, however, only a fraction of the thickness of the initial channel. Depending on the deepwater system, deposition of the condensed sections can be modeled following deposition of each channel-lobe feature or following several stacked channel-lobe events. A varying degree of stochasticity is incorporated wherever deemed suitable to simulate the randomness in the modeling approach.

Implementation Issues

A Fortran program is written to implement this deepwater-reservoir modeling approach. There are two major data structures maintained in the program: (1) a local data structure for the current bathymetry (as it exists at any arbitrary time) for the channel, lobe, and condensed-section placement as detailed in previous sections; and (2) a global data structure for stacking and updating the model as it is being built successively. The local data structure comprises several 2D arrays. The 2D arrays include those for initial bathymetry, bathymetry after channel erosion, bathymetry after channel-lobe deposition, bathymetry after condensed-section deposition, sediment-flow-vector azimuth, sediment-flow-vector slope, sediment-flow-vector pointers, contributing area, and reservoir-element identifiers. Once the modeling of a single channel-lobe and condensed-section event is completed, three bathymetric surfaces (top surface of condensed-section, top-surface of channel-lobe surface, and post-channel-erosion surface) and reservoir element identifiers are stored in separate 2D arrays of the global data structure. The same local data structure is used for the subsequent depositional events.

After modeling a specified number of depositional events (n_e as specified in the input section discussed later), a final 3D array defining the model is constructed from top-to-bottom. The reason for the top-to-bottom approach is the fact that younger events may erode older surfaces. The final 3D geometry data are stored in the corner-point geometry format. Horizontal positions of the cells are thus fixed; however, the vertical (bathymetric) z values will vary depending on the modeling of the depositional events. The vertical thickness of a grid cell can be as small as zero corresponding to no deposition in the cell. This is another important feature of this approach that is distinctly different from most reservoir modeling methods. The storage requirement within the program may seem redundant, but it allows great flexibility in the program such as high vertical resolution of the models and stratigraphic ordering.

Input Data

The important input data used in the modeling are summarized here. Horizontal model dimension is determined by n_x and n_y (number of grid cells) and grid size d_x and d_y in X and Y direction, respectively. Any unit system can be used, however, consistency of the unit system should be maintained. The initial bathymetry data have X, Y and Z values in a bathymetry data file in GEOEAS/GSLIB format. There should be n_x x n_y data in the bathymetry data file. The number of depositional events (channel-lobe) to be modeled is specified. A random number seed is input for introducing a varying degree of stochasticity. Channel-entry point (azimuth) data are specified for identifying source location position for each channel-lobe depositional event. Three values of azimuth (minimum, mode and maximum) are given for each depositional event. This specifies the triangular distribution from which one azimuth value is randomly drawn. Starting thickness and starting width-to-thickness aspect ratio for each channel-lobe depositional event are specified. Similar to source-direction data, triangular distributions specifications are input. Downdip-channel aspect-ratio increase factor and channel width increase factor are also specified.

Output

The outputs of the modeling program are presented in this section. A 3D model of the channel-lobe, and condensed section deposits is generated in corner-point geometry (ECLIPSE format[13]) format. Active cells in the reservoir as used in ECLIPSE are output. Facies identifiers are output (Shale – 0,3, Channel -1, and Lobe – 2) in ECLIPSE property file format. For initial bathymetry and after each channel-lobe, and condensed section depositional event, a number of parameters are

generated particularly for debugging and critical analysis. These parameters include sediment-flow vector and pointer, post-erosion, post-deposition, post condensed section bathymetry, reservoir element identifiers, and contributing areas. All of these are generated in a unified file in GEOEAS/GSLIB format. The 3D model files can be easily used in 3D visualization or reservoir simulation packages.

Modeling Example

We present an application of the approach for deepwater reservoir modeling. A 6.5 x 6.0 square kilometer area is gridded into 650 x 600 areal grid cells. Each cell dimension is 10 m x 10 m. The initial bathymetry is shown in Fig. 7A. In this example, there is a basin in the middle portion of the area that could represent an intraslope basin. We modeled 14 channel-lobe and condensed-section events in this example. The variations in azimuths for channel-entry points, updip channel thickness, and width-to-thickness aspect ratio for all events are shown in Tables 2, 3 and 4 (Appendix), respectively. For every event, updip-to-downdip width and width-to-thickness aspect ratio increment factors are

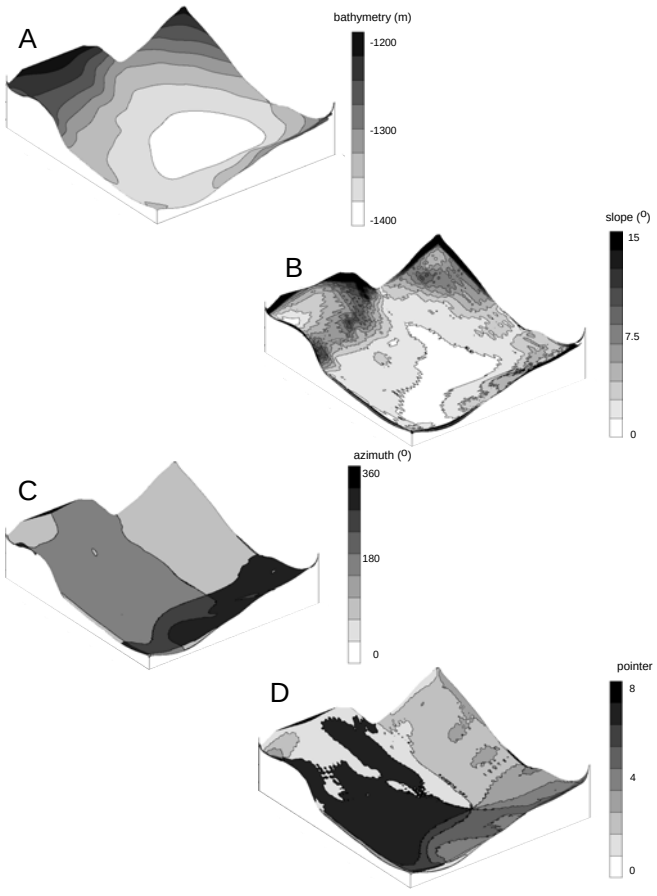

Figure 7: Maps of A) initial bathymetry, B) slope of the sediment-flow vector, C) angle of the sediment-flow vector, and D) pointer for the simple example discussed.

2.5 and 3.0, respectively. Along a channel trajectory, where the gradient reaches a value of 1.75°, erosion terminates and the channel becomes completely depositional. For the initial surface, the sediment-flow vector slope and azimuth and the corresponding pointer maps are shown in Fig 7.

Fig. 8 illustrates the 3D model for all 14 modeled events. Three cross sections (AA', BB', and CC') show the proximal, intermediate, and distal stacking patterns of the channel-lobe and condensed section events (Fig. 9). The proximal cross section, AA' (Fig. 9), clearly shows compensational channel stacking and the erosion surfaces. The net-to-gross ratio is highest in this intersection. The intermediate cross section, BB', reveals a lower degree of erosion/scour and lower net-to-gross

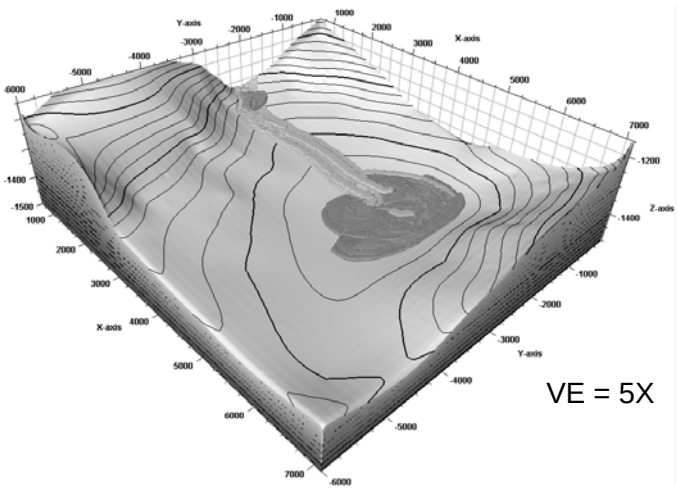

Figure 8: 3D view of the 14 channel-lobe events modeled in the simple example discussed.

ratio. The degree of confinement decreases at this location compared to the proximal location. The distal cross section, CC', shows the sheet-form nature of the reservoir architecture. Also evident is the lower net-to-gross ratio in the distal region. A longitudinal cross section, DD', illustrates the continuity patterns of the architecture. A high degree of discontinuity is evident in the updip region due to channel erosion and sinuosity (Fig 9, left side of DD'). Continuity increases in the downdip region particularly with the deposition of wider channels and sheet-form lobes. The updip-to-downdip thickness decrease is also evident in this longitudinal intersection. The modeled architectural features are also in agreement with conceptual geological views of the deepwater reservoir architectures[14,15,16].

Importantly, this reservoir modeling approach attempts to mimic the conceptual depositional and erosional processes in deepwater settings unlike purely stochastic approaches. Through this modeling process, realistic deepwater reservoir architectures are produced. The motivation for this approach was to incorporate both stratigraphic and geomorphic information, conceptual and quantitative. Through this modeling approach, it is possible to quantify the tortuosity, curvature, gradients,

bathymetric change, and a number of other parameters for channel bodies and corroborate those with our understanding of these systems. It is also possible to control these parameters in the modeling approach. An important advantage of this approach is that it is computationally efficient. For the modeling example demonstrated above (grid cells 650 x 600 x 28), the CPU time on a modern desktop computer is less than 3 minutes. Of course, the CPU time increases with the model dimensions. The other major advantage is that the outputs are generated in multiple formats (corner-point geometry format, GEOEAS/GSLIB format) and can easily be used in modeling, visualization, and fluid-flow simulation packages. Well and seismic data conditioning are being developed. The combination of the corner-point geometry format and the modeled depositional surfaces facilitates horizon modeling and thus separate horizon modeling is not required.

Limitations

A number of geomorphic parameters and concepts, other than those stated in this paper, could be incorporated in the modeling process. These include erodability index[17], Strahler's network ordering (relates stream ordering in terms of network architecture[18]), Horton's laws (regarding distributions of stream lengths[19]), Hack's law (relates basin length to basin area[20]) and others. The simulation of deepwater reservoir elements, particularly lobe forms, could be improved by incorporating the above concepts. Additional observations from flume studies, geological process experiments, outcrop, and stratigraphic studies will augment future modeling attempts.

Methods are being developed to condition the deepwater reservoir models to well and seismic data. Other modifications to incorporate deepwater reservoir architectural elements such as levees (channel-levee deposits) and sub-facies within depositional settings will also be explored.

Conclusions

This deepwater-reservoir modeling approach constructs realistic 3D reservoir architectures and models. This computationally efficient modeling technique will lend itself for use in large-scale real-time reservoir modeling and inversion problems. This method incorporates both stratigraphic and geomorphic constraints. This modeling approach retains the flexibility of the stochastic approaches as well as the essence of geological process-based modeling approaches.

This reservoir modeling approach attempts to mimic the conceptual depositional and erosional processes in deepwater settings unlike some purely stochastic approaches. Through this modeling approach, it is possible to quantify the tortuosity, curvature, gradients, bathymetric changes, and a number of other parameters for channel bodies and corroborate those

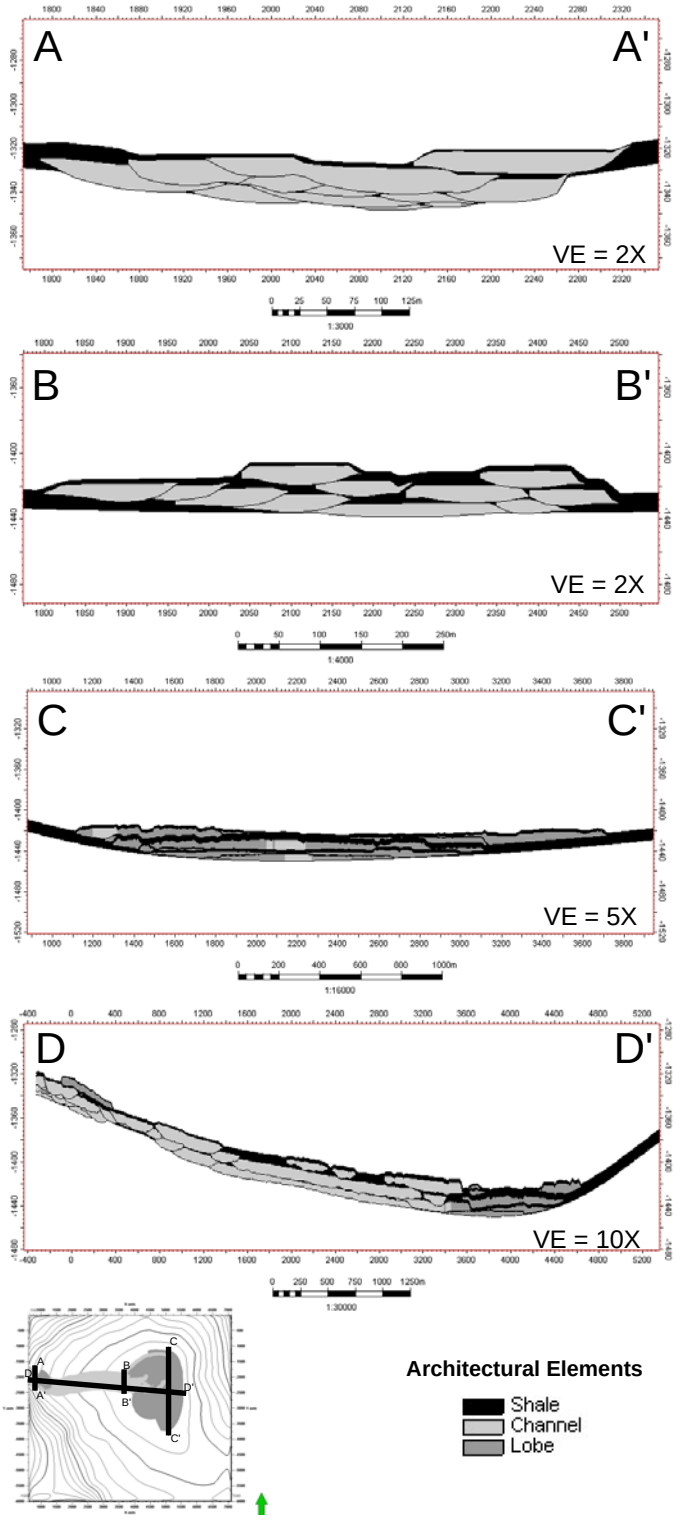

Figure 9: Cross sections that illustrate the reservoir architecture of the channel-lobe and condensed section events of the simple example. The cross sections highlight the stacking patterns and architecture for proximal, intermediate, and distal locations and longitudinal to the primary direction of deposition. The proximal cross section, AA', shows compensational channel stacking and the erosion surfaces. The intermediate cross section, BB', reveals a lower degree of erosion/scour and lower net-to-gross ratio compared to section A-A'. The distal cross section, CC', shows the sheet-form nature of the reservoir architecture. A longitudinal cross section, DD', illustrates the continuity of the reservoir architecture. VE=vertical exaggeration.

with our expert knowledge. The approach is computationally efficient. The other major advantage is that the outputs are generated in multiple formats and can easily be used in modeling, visualization, and fluid-flow simulation packages.

Acknowledgements

This research is funded through a grant from the American Chemical Society, Petroleum Research Fund and through the Energy and Minerals Applied Research Center at the University of Colorado at Boulder.

References

1. Deutsch, C. V. & Journel, A.: *GSLIB: Geostatistical software library and user's guide*. Oxford University Press, New York, 2nd Edition (1998).

2. Strebelle, S., & Payrazyan, K.: "Modeling of a deepwater turbidite reservoir conditional to seismic data using multiple-point geostatistics": SPE Paper 77425, presented at the 2002 SPE Annual Conference and Technical Meeting, San Antonio, Texas, October 6-10.

3. Haldorsen, H. H. & Lake, L. W.: "A new approach to shale management in field-scale model": *SPE Journal*, (April 1984), 447-457.

4. Haldorsen, H. H. & Chang, D. W.: "Notes on stochastic shales, from outcrop to simulation model", in *Reservoir Characterization*: London, Academic Press (1986) 445-485.

5. Deutsch, C. V. & Tran, T. T.: "FLUVSIM: A program for object-based stochastic modeling of fluvial depositional systems": *Computers and Geosciences*, **28** (2002) 525-535.

6. Deutsch, C. V, Xie, Y. & Cullick, S.: "Surface geometry and trend modeling for integration of Stratigraphic data in reservoir models", SPE Paper 68817, presented at the 2001 SPE Western Regional Meeting, Bakersfield, California, March 26-30.

7. Pyrcz, M. J., Catuneanu, O., & Deutsch, C. V.: "Stochastic Surface-based Modeling of Turbidite Lobes": *AAPG Bulletin*., **89**, 2 (2005) 177-191.

8. Tetzlaff, D. A., & Harbaugh, J. W.: *Simulating clastic sedimentation*, van Nostrad Reihnhold, New York (1989) 202.

9. Martinez, P. A., & Harbaugh, J. W.: *Simulating near-shore environments*, Pergamon Press, New York (1993) 265.

10. Tarboton, D. G.: "A new method for the determination of flow directions and contributing areas in grid digital elevation models": *Water Resources Research*, **33**, 2 (1997) 309-319.

11. Weimer, P. & Slatt, R. M.: *Petroleum Systems of Deepwater Settings*, 2004 Distinguished Instructor Short Course, SEG, EAGE, Tulsa, Oklahoma (2004).

12. Mutti, E. & Normark, W. R.: "An integrated approach to the study of turbidite systems", in P. Weimer and M. H. Link, eds, *Seismic facies and sedimentary processes of submarine fans and turbidite systems*: Springer-Verlag, New York (1991) 75-106.

13. GeoQuest.: *ECLIPSE Reference Manual*, Schlumberger, Houston, U.S.A (2004).

14. Beaubouef, R. T., Rossen, C., Zelt, F. B., Sullivan, M. D., Mohrig, D. C. & Jennette, D.: *Deepwater sandstones, Brushy Canyon Formation, west Texas: Field guide*, AAPG Hedberg Field Research Conference (1999).

15. Beaubouef, R. T., Abreu, V. & Van Wagoner, J. C.: "Basin 4 of the Brazos-Trinity slope system, western Gulf of Mexico: The terminal portion of a late Pliestocene lowstand systems tract", in H. H. Roberts, N. C. Rosen, R. H. Fillon, and J. B. Anderson, eds. *GCS-SEPM Foundation 23rd Annual Bob F. Perkins Research Conference* (2003).

16. Johnson, S. D., Flint, S., Hinds, D., & DeVille Wickens, H.: "Anatomy, geometry and sequence stratigraphy of basin floor to slope turbidite systems, Tanqua Karoo, South Africa": *Sedimentology*: **48** (2001) 97-1023.

17. Tarboton, D. G.: "Terrain analysis using digital elevation models in hydrology", in *23rd ESRI International Users Conference*, San Diego, California, July 7-11 (2003).

18. Strahler, A. N.: "Hypsometric (area-altitude) analysis of erosional topography": *Geological Society of America Bulletin*, **63** (1952) 1117-1142.

19. Horton, R. E.: "Erosional development of streams and their drainage basins; hydrophysical approach to quantitative morphology", *Bulletin Geol. Soc. Am.*: **56** (3) (1945) 275-370.

20. Hack, J. T.: "Studies of longitudinal stream profiles in Virginia and Maryland", *US Geological Survey Prof. Pap.*: **294-B**, (1957) 45-97.

Appendix

Event	Channel-entry point azimuth (radian)		
	Minimum	Mode	Maximum
1	5.00	5.02	5.05
2	4.96	4.97	4.99
3	5.04	5.06	5.10
4	4.97	5.01	5.04
5	5.06	5.09	5.13
6	4.93	4.95	4.97
7	5.09	5.12	5.15
8	5.02	5.05	5.07
9	4.96	4.97	4.99
10	4.93	4.95	4.97
11	5.05	5.07	5.11
12	4.97	5.01	5.04
13	4.92	4.94	4.96
14	5.02	5.05	5.08

Table 2: Input variation in channel-entry point azimuth in a triangular distribution form (minimum, mode and maximum define the triangular distribution).

Event	Initial channel thickness (m)		
	Minimum	Mode	Maximum
1	9.15	10.20	11.25
2	9.65	9.70	10.75
3	9.15	11.20	12.25
4	10.15	11.20	12.25
5	11.25	12.30	14.35
6	10.15	12.20	13.25
7	9.15	10.20	11.25
8	8.15	9.20	10.25
9	8.15	9.20	10.25
10	9.15	10.20	11.25
11	10.15	12.20	13.25
12	11.15	11.20	12.25
13	10.15	10.20	10.25
14	11.15	11.20	11.25

Table 3: Input variation in initial channel thickness in a triangular distribution form (minimum, mode and maximum define the triangular distribution).

Event	Initial channel width-to-thickness aspect ratio		
	Minimum	Mode	Maximum
1	8.15	9.20	10.25
2	9.65	10.70	11.75
3	10.15	11.20	12.25
4	11.15	12.20	13.25
5	10.25	11.30	12.35
6	9.15	10.20	11.25
7	8.15	9.20	10.25
8	9.15	10.20	11.25
9	10.15	11.20	12.25
10	9.65	10.70	11.75
11	10.15	10.20	10.25
12	11.15	11.20	11.25
13	10.25	10.30	10.35
14	10.15	10.20	10.25

Table 4: Input variation in initial channel width-to-thickness aspect ratio in a triangular distribution form (minimum, mode and maximum define the triangular distribution).